Silicon nitride membrane mirrors for focus control
by Robert Andreas Friholm

A thesis submitted in partial fulfillment of the requirements for the degree of Masters of Science in Electrical Engineering
Montana State University
© Copyright by Robert Andreas Friholm (2001)

Abstract:
This thesis is an investigation into the feasibility of using deformable silicon nitride membrane mirrors for focus control without introducing spherical aberrations. The mirrors are circular with sizes ranging from 300pm to 1500pm diameter. Focus control is achieved by deflecting the membranes, while maintaining a parabolic surface shape, as not to introduce spherical aberrations. The deflection of the membranes is done electrostatically and uses two concentric actuation zones for spherical aberration control. Variation in the membrane boundary conditions was investigated to determine the effect on spherical aberration in the mirrors. The devices were built using a method which is a hybrid between surface and bulk micromachining. The fabrication method enables the air gap beneath the membrane to be precisely controlled to the desired depth. Devices 1500 pm in diameter displayed focal length adjustments ranging from infinity to 39mm, corresponding to membrane displacement of 3.6 pm at membrane center.

It was shown that spherical-aberration-free focus control was possible to achieve using the two-actuation-zone configuration. The devices were found to have resonant frequencies in the 20-25kHz range, which makes the devices suitable for real time video rate focus control. Integration of a device into a confocal microscope with object space numerical aperture yielded a change in focal plane location of 75 pm, with insignificant impact on system performance. It was therefore concluded that the devices are suitable for spherical aberration free focus control at relatively high frequencies.

SILICON NITRIDE MEMBRANE MIRRORS FOR FOCUS CONTROL

By

Robert Andreas Friholm

A thesis submitted in partial fulfillment
of the requirements for the degree

of

Masters of Science

in

Electrical Engineering

MONTANA STATE UNIVERSITY
Bozeman, Montana

August 2001

N378
F9164

APPROVAL

of a thesis submitted by

Robert Andreas Friholm

This thesis has been read by each member of the thesis committee and has been found to be satisfactory regarding content, English usage, format, citations, bibliographic style, and consistency, and is ready for submission to the College of Graduate Studies.

David Dickensheets
Committee Chair
(Signature) David L. Dickensheets
(Date) Aug 14, 2001

Approved for the Department of Electrical & Computer Engineering

Jim Peterson
Department Head
(Signature) James N. Peterson
(Date) 8/21/01

Approved for the College of Graduate Studies

Bruce McLeod
Graduate Dean
(Signature) Bruce R. McLeod
(Date) 8-24-01

STATEMENT OF PERMISSION OF USE

In presenting this thesis in partial fulfillment of the requirements for a master's degree at Montana State University, I agree that the Library shall make it available to borrowers under the rules of the Library.

If I have indicated my intention to copyright this thesis by including a copyright notice page, copying is allowable only for scholarly purposes, consistent with "fair use" as prescribed in the U.S. Copyright Law. Requests for permission for extended quotation from or reproduction of this thesis in whole or in parts may be granted only by the copyright holder.

Signature Robert Fricholm

Date 8/15/01

TABLE OF CONTENTS

1. INTRODUCTION 1

2. THEORETICAL DEVELOPMENT 5

Target Specifications 5
Parabolic Mirror 5
Mechanical Behavior 10
Membrane Actuation 11
Modeling 12

3. DESIGN 16

Material / Structural Choices / Fabrication Constraints 16
Proposed Device 17
  Boundary Conditions 18
  Actuation Regions 19
  Etch Holes 20
Secondary Concerns 21
Final Device Idea 22

4. MAKING THE DEVICES 23

Process Flow 23
  Considerations 26
  Layout 27
Release Process 30
  Considerations 31
  Imaging of Release Process 34
  Results Oxide Etch 35
  Results Silicon Etch 39
Summary 42
Recommendations 43

5. RESULTING DEVICES 44

Optical Profilometer 44
  Profilometer Setup 45
  Profilometer Measurement / Post-processing 46
  Optical Profilometer Results 47
Dynamic Measurements 53
Device Issues 58

TABLE OF CONTENTS - CONTINUED

6. INTEGRATION INTO MARS PROBE....60

Mars Probe Setup....60
Benchtop Integration....61
Miniature Probe Integration....64
Theoretical Treatment....64
Integration....67
Summary....69

7. CONCLUSIONS....72

BIBLIOGRAPHY....75

LIST OF TABLES

Table Page

2-1. Results from FEA simulations on 1500μm device with segmented and thinned support....................15

5-1. Obtained f_0 and Q values of various devices from curve fits of dynamic response data from device with 12μm pit depth................57

LIST OF FIGURES

Figure Page

2-1. Imaging of a collimated beam by a
a) Spherical reflector
b) Parabolic reflector 6

2-2. Incident collimated beam on spherical reflector and thin lens
a) Collimated beam is imaged at focal point of spherical reflector
b) Collimated beam is imaged at focal point of thin lens 7

2-3. Radius of spherical reflector as function of device radius and deflection 8

2-4. Resulting focal length of 750μm and 1500μm diameter device from deflection at center of device 9

2-5. Finite element model of membrane structure 13

2-6. FEA simulation results from actuation of 1500μm device by pressure on inner, outer, and both actuation zones 15

3-1. Conceptual cross-sections of polysilicon device (surface micro-machining) and silicon nitride device (hybrid between surface and bulk micromachining) 17

3-2. Design layout of a 300μm diameter device with 10% duty width and weakened edge support 19

4-1. Fabrication sequence for the membrane mirrors 25

4-2. Mask layers of the membrane mirrors 28

4-3. SEM picture of 1500μm device with segmented but no thinning of the edge support 29

4-4. SEM images of membrane devices illustrating key features
a) Lateral etch-stop and thinned support of circular device
b) Metal trace crossing back-filled etch stop trench
c) Close-up of thinned edge support
d) Segmented thinned support of broken square device 30

LIST OF FIGURES - CONTINUED

Figure Page

4-5. Setup for imaging of silicon etching process....35

4-6. SEM image of broken device, illustrating where
devices with thinned edge support break....36

4-7. Crack in membrane structure terminating in etch hole....36

4-8. Wave propagating across 1000μm 10% device as
pillars beneath membrane are etched away
a) Wave propagates from perimeter of device
b) Wave reaches center actuation zone
c) Amount of remaining pillars is less than
diameter of center actuator
d) Device is freestanding....38

4-9. Frames from video of TMAH silicon etch (up is to the left)
a) Steady stream of bubbles coming out of a few vias
b) Stream of bubbles cease
c) Large bubble is forming beneath membrane
d) Explosive burst, releasing hydrogen bubbles....40

4-10. SEM images illustrating bottom profile of different devices
a) Bottom of pit beneath device with segmented support
b) Device with continuous support....42

5-1. 1500μm 10% membrane with no thinning of edge support
a) Perfectly flat die with 200v applied to both actuation zones
b) Tilted membrane (to give straight lines across it), 0v applied
c) Tilted membrane, 200v applied to both actuation zones 45

5-2. Optical profilometer setup using a Mireu interferometer
objective lens 46

5-3. Deflection vs. Applied Voltage graph of a 1500μm device
with 10% duty width , no thinning of the edge support,
and 12μm pit depth 48

5-4. Surface profile data and curve fit of 1500μm 10% device
without thinned edge support, with 0v and 200v applied
on both actuation zones....50

LIST OF FIGURES - CONTINUED

Figure Page

5-5. Images of 1500μm 10% device with no thinning of edge support
a) Actuation voltages: 150v on inner actuation zone, 0v on outer
b) Actuation voltages: 0v on inner actuation zone, 150v on outer
c) Actuation voltages: 150v on both actuation zones 51

5-6. Surface profile data and curve fit of 1500μm 10% device without thinned edge support, with 150v applied to inner, outer, and both actuation zones..51

5-7. Actuation voltage pairs where spherical aberration goes through zero point..53

5-8. Data from dynamic response measurement and low pass curve fit of 1500μm 10% device. curve fit gave f_0 = 19.3khz and q = 0.4977 54

5-9. Data from dynamic response measurement and low pass curve fit of 1500μm 100% device. curve fit gave f_0 = 22.3khz and q = 0.503 55

5-10. Data from dynamic response measurement and low pass curve fit of 300μm 10% device. curve fit gave f_0 = 25.9khz and q = 0.564 55

5-11. Second order low pass curve fit to dynamic response measurements of 1500μm 10%, 1500μm 100%, and 300μm 10% devices without thinning of support.................................56

5-12. Graph of leakage current as function of applied voltage on a bonding pad (which is not connected to a device) 58

6-1. Optical setup of benchtop CMaRS integration 61

6-2. Images obtained at focusing extremes of 750μm membrane
a) 0v applied to membrane (no deflection)
b) 200v applied to membrane (1.2μm deflection)..............................63

6-3. Miniature system with membrane mount integrated 64

LIST OF FIGURES - CONTINUED

6-4. Lens configuration of miniature probe 65

6-5. Focus control of miniature system as a function of center deflection of incorporated 1500μm device (paraxial case)..................66

6-6. Membrane mount for integration into CMaRS probe
a) Mount with small die containing two 1500μm devices
b) Wire-bonds from 0Ω resistors to bonding pads of 1500μm 10% device 67

ABSTRACT

This thesis is an investigation into the feasibility of using deformable silicon nitride membrane mirrors for focus control without introducing spherical aberrations. The mirrors are circular with sizes ranging from 300μm to 1500μm diameter. Focus control is achieved by deflecting the membranes, while maintaining a parabolic surface shape, as not to introduce spherical aberrations. The deflection of the membranes is done electrostatically and uses two concentric actuation zones for spherical aberration control. Variation in the membrane boundary conditions was investigated to determine the effect on spherical aberration in the mirrors. The devices were built using a method which is a hybrid between surface and bulk micromachining. The fabrication method enables the air gap beneath the membrane to be precisely controlled to the desired depth. Devices 1500μm in diameter displayed focal length adjustments ranging from infinity to 39mm, corresponding to membrane displacement of 3.6 μm at membrane center. It was shown that spherical-aberration-free focus control was possible to achieve using the two-actuation-zone configuration. The devices were found to have resonant frequencies in the 20-25kHz range, which makes the devices suitable for real time video rate focus control. Integration of a device into a confocal microscope with object space numerical aperture yielded a change in focal plane location of 75μm, with insignificant impact on system performance. It was therefore concluded that the devices are suitable for spherical aberration free focus control at relatively high frequencies.

CHAPTER 1

INTRODUCTION

The first Microelectromechanical system (MEMS) device was made in the mid-1960s, when a resonating MOS gate structure was built at Westinghouse [1]. It was not until the late 1980s that the field of MEMS started gaining ground and the term MEMS, itself, was not officially adopted until 1989 [2]. Since then, significant advancements have been made in the area. The main reason for the fast development of the technology is that MEMS uses existing CMOS technology that has evolved over the last decades with the rapid development of the microprocessor and memory industry [3]. As the minimum feature size of MEMS structures normally is around a few microns, older CMOS equipment can be used, which lowers production cost. Since MEMS devices can be produced by batch processing, large volumes can be produced at low cost per individual device.

Silicon has very good material properties (comparable to steel) and very durable and versatile structures can be constructed from it. MEMS processes are CMOS compatible, which makes it possible to create a monolithic integration with mechanical and microelectronic parts on the same chip and reduce the part size of the system.

The ability to create mechanical structures with or without integrated electronics on a small scale using silicon wafers has vast benefits in several applications. The automotive industry, which has been the driving force behind the sensor technology of

MEMS, uses MEMS accelerometers to control deployment of airbags. Because of the small size and relatively low cost of the devices redundant sensors can be installed for increased reliability with low overhead.

The information technology industry is another major contributor to the growth of MOEMS technology (Micro-opto-electromechanical systems). As fiberoptic communication has grown with the expansion of the internet, small and reliable MOEMS devices can be used in applications such as fiberoptic switches to reroute incoming optical signals to any of a number of outgoing fibers.

Considerable attention has been dedicated to the development of adaptive optics using MOEMS technology. The bulk of the adaptive optics is focused on correcting for random aberrations in applications such as ground based telescopes used in astronomy, where Earth's atmosphere introduces random aberrations [4, 5]. These are complex devices with large grids of actuators that control the surface shape of the mirrors. Some devices are focused on correcting for one specific type of aberration and can therefore use simple mirror shapes that are already known. These devices generally correct for one of the primary (Seidel) aberrations of a system such as defocus [6, 7, 8, 9], spherical aberration, and astigmatism [10]. Using compensating adaptive optics, correcting for known aberrations, will enable cheaper lenses of lower optical quality to be utilized in optical systems at a lower cost, but with performance comparable to more expensive systems.

In this thesis, deformable mirrors for focus control are presented. Previous efforts toward focus control have been made based on a number of different concepts. Burns and Bright [7] designed a thermally controlled focusing mirror capable of frequencies beyond 120Hz with a maximum power consumption of 480mW. Concentric rings of aluminum on the polysilicon membrane surface acts as a reflector and the largest ring, when resistively heated, causes the membrane curvature to change due to the change in residual stress of the materials. Zhu and Sun [6] demonstrated aberration free focusing using a 19-channel deformable silicon nitride membrane mirror with a diameter of 1cm. The bottom of the membrane structure has 19 independent hexagonal actuation zones, which causes the aluminum-coated membrane to deflect due to electrostatic force caused by the applied voltages. A lookup table is used to control the voltages of the actuators below the mirror to maintain aberration free imaging at frequencies ranging up to hundreds of Hertz. Vdovin and Sarro [8] produced mirrors with a clear aperture of 1cm, capable of focal lengths ranging from ∞ (flat mirror) to 0.25m at frequencies up to 75Hz. A 19-channel actuation scheme similar to the one used by Zhu and Sun is employed by these deformable membrane mirrors. Derivations of these mirrors are now commercially available in sizes ranging from 5mm to 50mm, actuation schemes with 19 to 119 channels, and frequency responses of up to 500Hz.

Our devices are circular, low stress, silicon nitride membrane structures on the order of a millimeter in diameter that are suspended across a pit in the bulk silicon beneath it. They operate on the principle that a mirror with a cross sectional parabolic surface figure acts as a positive lens. By deflecting the mirror to varying degrees, the

level of curvature of the mirror changes, which moves the location of the focal point of the mirror. Two topside gold electrodes electrostatically control the amount of deflection of the mirrors and also make up the reflective surface of the mirrors. By adjusting the control voltages of the two independent actuation zones, the membranes can maintain zero spherical aberration. The target voltage range for surface control of the mirrors is below 200V for a deflection of a few microns, which yields a focal length range from ∞ to 0.04m. The devices have frequency responses in the 20-25kHz range, which makes them suitable for real time video rate focus control.

The mirrors are intended for integration into a confocal microscope and Raman spectrometer (CMaRS) probe that uses beam scanning to compose an image [11]. The probe will be attached to a robotic arm in a rover-based vehicle for Mars exploration. The robotic arm is used for moving the probe up to the sample. The final adjustment of the focal plane is performed by the adaptive optics of the probe, which enables the probe to image samples that are not perfectly flat by adjusting for optimal focus across the field of view of the sample. At this point the focus control of the probe is done by a lens-mount which is moved by a piezoelectric actuator. Integration of a deformable mirror would decrease the overall weight and size of the system and the low power consumption of an electrostatically controlled membrane mirror is ideal for applications with limited available power.

CHAPTER 2

THEORETICAL DEVELOPMENT

Target Specifications

A membrane device with a reflective surface with good optical quality is desired. In order to maintain spherical aberration free imaging, it needs to maintain a perfectly parabolic shape when deflected. Means of controlling the surface shape of the membrane to maintain a parabolic shape need to be implemented, as the device is expected to deviate from a perfectly paraboloidal shape under uniform pressure. The device is desired to be able to achieve a large enough deflection to give 200μm of focus control for a given system (discussed in chapter 6). The voltage required to achieve this actuation should ideally be less than 200V to avoid electric breakdown of the device.

Parabolic Mirror

In order to maintain an aberration-free imaging system with a membrane device, the surface shape of the membrane needs to be parabolic (assuming collimated incident illumination). This is illustrated in figure 2-1, where a spherical reflector and a parabolic reflector are shown together. In a) it is noted that the rays of a collimated beam do not come to a perfect focus, but are in fact spread around the focal point by the spherical mirror. This is known as spherical aberration. The incoming rays from the collimated

beam are reflected by the parabolic mirror in b) and come to a perfect focus at the focal point, f.

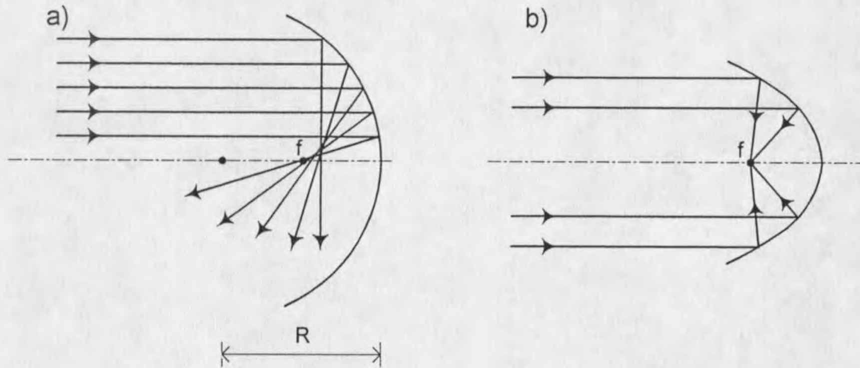

Figure 2-1. Imaging of a collimated beam by a
a) Spherical reflector
b) Parabolic reflector

For the paraxial case (rays close to the optical axis), a spherical reflector acts like a paraboloidal mirror of focal length f = R/2 (R is the radius of the spherical mirror). Figure 2-2 shows the concept of how a reflective spherical surface acts as a positive lens. The governing equation for imaging with a spherical mirror is

$$\frac{1}{z_1}+\frac{1}{z_2}=-\frac{2}{R}, \tag{2-1}$$

where z_1 is the distance from the mirror to the object, z_2 is the distance from the mirror to the image, and R is the radius of the mirror. The conventions of the formula are as shown in figure 2-2 a). The minus sign of the radius denotes a concave mirror. For a thin lens, the corresponding equation is

$$\frac{1}{z_1}+\frac{1}{z_2}=\frac{1}{f}, \tag{2-2}$$

where z_1 is the distance from the lens to the object, z_2 is the distance from the lens to the image, and f is the focal length of the lens. The conventions of the formula are as displayed in figure 2-2 b).

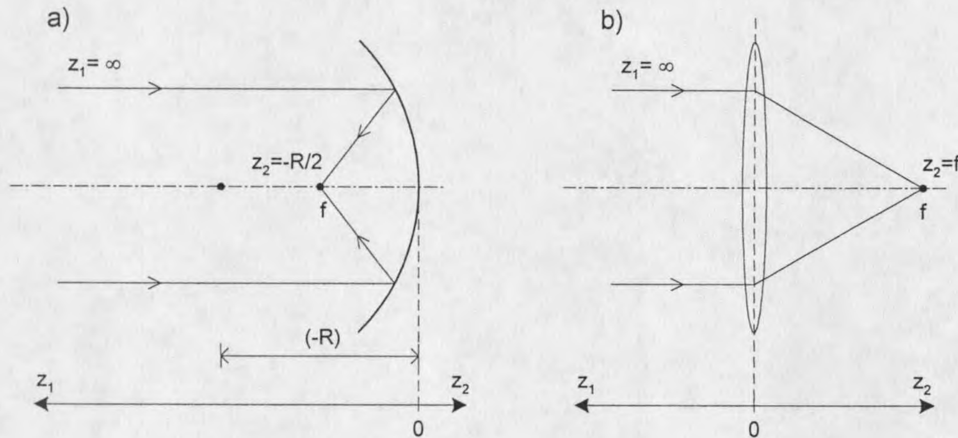

Figure 2-2. Incident collimated beam on spherical reflector and thin lens.
a) Collimated beam is imaged at focal point of spherical reflector.
b) Collimated beam is imaged at focal point of thin lens.

Since z_1 is at infinity for the two cases shown above, the location of the image is found to be at R/2 for the spherical mirror, and at f for the thin lens. The radius of (2-1) depends on the radius and the amount of deflection of the device. Figure 2-3 shows how the radius of the spherical mirror was derived from the deflection and radius of the membrane device. The formula for the radius of the spherical mirror (R) is

$$R = \frac{d^2 + r^2}{2d} \approx \frac{r^2}{2d} \text{ for } d \ll r, \qquad (2\text{-}3)$$

where d is the deflection and r is the radius of the device in question.

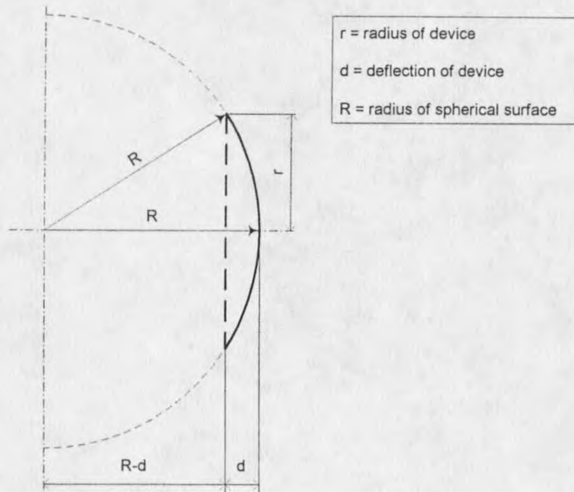

Figure 2-3. Radius of spherical reflector as function of device radius and deflection.

The resulting focal length as a function of center deflection of a device is shown in figure 2-4 for a 750μm and a 1500μm diameter device. Since the devices are assumed to be perfectly flat when no pressure is applied, the focal length of the membranes will be infinite at 0 deflection. The same amount of center deflection of devices of varying size will give different focal lengths. Assuming the same level of deflection for devices, the smaller the device is, the shorter its focal length will be. The focal length will change more rapidly with the initial deflection for a smaller device. This will result in a greater range of focus adjustment for small deflections of smaller devices.

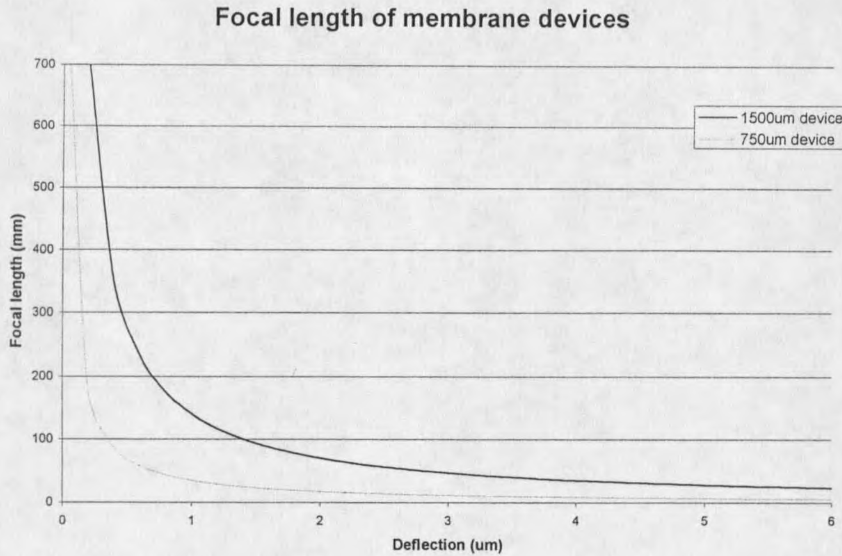

Figure 2-4. Resulting focal length of 750μm and 1500μm diameter device from deflection at center of device.

Since a paraboloidal shape is desired to obtain a perfect focus, the surface profile of the deflected membrane will have a deflection, which is proportional to the square of the position away from the center of the membrane. Any deviation from perfect r^2 dependence will therefore cause a non-parabolic shape and thereby introduce aberrations to the system in which it is being used. In order to evaluate the performance of the membrane, its surface shape will be fit to a polynomial of the form

$$y=a_2r^2+a_4r^4, \qquad (2\text{-}4)$$

where y is the deflection of the membrane at a the radial location r. The a_2 coefficient shows the parabolic shape of the membrane (focal point location) and the a_4 coefficient shows the amount of spherical aberration introduced by the membrane. The focal length of the parabolic mirror is given by

$$f = \frac{1}{4a_2} \qquad (2\text{-}5)$$

Higher order aberrations will be neglected, as the spherical aberration is the dominating aberration due to non-parabolic surface shape of the devices. The maximum spherical aberration of the device in waves is given as

$$W_{Spherical} = \frac{2a_4 r^4}{\lambda}, \qquad (2\text{-}6)$$

where r is the device radius and λ is the light source wavelength.

Mechanical Behavior

The mechanical behavior of the device needs to be such that when pressure is applied to it, the surface shape of the devices will be close to parabolic. The natural shape of a membrane under uniform pressure is parabolic [4], so it is desirable to have the device acting as a mechanical membrane. If the device acts more like a clamped plate, the surface shape under uniform pressure will not be parabolic due to the rigid boundary conditions of the plate.

The difference between membrane behavior and plate behavior for small deflections is dependent upon the initial tensile load of the device. When the tensile load is zero, the device behaves like a classical plate. As the tensile load increases, the behavior goes toward that of a membrane. The device goes toward pure membrane behavior as the tensile load goes towards infinity [12].

For the discussed devices, the tensile load is caused by the residual stress of the silicon nitride layer. If the residual stress of the device is increased, the resonant frequency is increased and the parabolic surface shape of the device is improved [9].

Since the residual stress is a key part of the restoring force of the device, an increase in the residual stress will increase the pressure needed to deflect the device.

Membrane Actuation

In order to deflect the membrane, reflective gold actuators are deposited on top of the membrane. In addition to being a highly reflective surface and acting as a mirror, the layer is used to deflect the membrane by means of electrostatic control. By grounding the silicon substrate beneath the device, it acts as a counter electrode to the gold layer on top of the devices when a voltage is applied to it. The deflecting force (F) acting upon the device as a result of the voltage differential is defined as

$$F = \frac{\varepsilon_r \varepsilon_0 V_c^2 S}{2d^2}, \qquad (2\text{-}6)$$

where ε_0 is the dielectric constant of vacuum, ε_r is the relative dielectric constant of the material between the electrodes, V_c is the applied control voltage, S is the area of the electrode, and d is the distance between the plates. Because of the aspect ratio between the device radius and the gap beneath the structure as well as the small distance between the membranes and the substrate, large forces can be obtained with relatively small control voltages. Since the available range of control voltages remains the same independent of device size, the larger devices will have greater force acting on them since the surface area increases. The larger devices will therefore achieve greater deflections than the smaller devices. However, a smaller device achieves a higher level of curvature for small deflections (and therefore a shorter focal length).

To achieve greater control of the surface shape of the deflected membrane, an actuator scheme with a center circle and an outer annular ring was implemented on top of the membrane structure (chapter 3). Simulations showed that it would be possible to minimize the a_4 term of the deflected device, thereby achieving a perfectly parabolic shape, using this actuation scheme.

Modeling

In order to understand how the device would react to different structural configurations and varying pressure, finite element analysis (FEA) of simple plate models of the devices was performed (code by Phil A. Himmer and B. Jeff Lutzenberger). The parameters investigated were different pressure zones, varying edge support models with the options of segmented support, and a thinned edge support ring around the perimeter of the devices.

Because of the radial symmetry of the device, the FEA model was composed of a 36° radial piece of the entire device. Figure 2-5 shows the layout of the model. It has two separate pressure zones that are marked as "Inner" and "Outer" in the figure and represent where the different actuation zones will be located. These zones have different grid sizes in the model. The outer zone has a finer grid than the inner as the change in displacement will be smaller there and more resolution is necessary. The inner pressure zone is twice as large (radially) as the outer zone, which is shown in the figure as it being $^2/_3$ of the radius and the outer zone makes up $^1/_3$ of the total radius. The device of the figure has a segmented edge support with 10% duty width, where the nitride strips are located every

36°. Consequently, the support strips being shown in the picture, are actually only half of an edge support strip. The support also has a thinned region in the edge support of the device, which will yield a more membrane-like pressure response of the devices. The residual stress of the device was integrated into the model as a change in temperature of the structure.

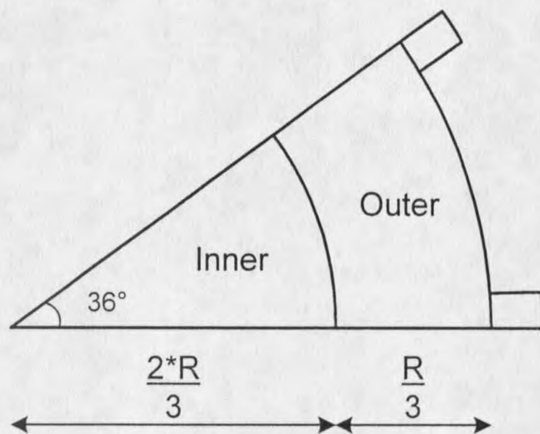

Figure 2-5. Finite element model of membrane structure.

The device was modeled as a silicon nitride plate with a thickness of 0.5μm, and 0.1μm at the thin portion of the edge support. The material properties of the devices were given to be 290GPA for the Young's modulus and 0.24 for the Poisson's ratio. By applying a uniformly distributed pressure to each of the pressure zones (the electrostatic force of each zone which will arise from applied voltages), surface shape was simulated.

The impact of the two different actuation zones was tested by applying pressure to one actuation zone at a time and then both actuation zones at once. The test was carried out on a variety of device sizes, with center deflections ranging up to 7μm. the resulting deflection was post-processed in Matlab to find the surface shape of the membrane. The

data was fitted to a function of the form $r^2a_2 + r^4a_4$ (2-4) to know the amount of focus control and aberrations.

The simulations of a 1500μm device with segmented and thinned edge support gives a representative view of the results of the simulations. The membrane was deflected to 7μm at the center of the device by pressure on the outer, inner, and both actuation zones respectively. The resulting data of the simulations are presented in table 2-1. Figure 2-4 shows the resulting surface figures corresponding to the values of table 2-1. The a_2 and a_4 coefficients and the peak error of the curves were calculated using the central 80% of the devices. The peak error is defined as the maximum deviation by the membrane shape from the best-fit curve fitted a_2r^2 shape. It could consistently be shown that spherical wavefront errors (caused by deviation from parabolic surface shape) were less than $\lambda/10$ at 852nm wavelength for pressure on the outer actuation zone. Because of the small magnitude of the error, it was concluded that aberration free imaging would be possible. The resulting surface figure curves are shown together with a parabolic curve in figure 2-4. The best fit to a parabola was obtained by pressure on the outer actuation zone. Uniform pressure provides the second best fit and pressure on the inner actuation zone has the highest deviation from the quadratic function. The simulations showed that the surface shape of the membrane could be controlled by applying different pressure to the two actuation zones.

Table 2-1. Results from FEA simulations on 1500μm device with segmented and thinned support.

Actuation Zone	a2	a4	Peak Error (μm)	Peak Error (λ)
Inner	-1.90E-05	1.30E-11	0.38	0.45
Outer	-1.31E-05	6.26E-13	0.04	0.04
Both	-1.60E-05	6.75E-12	0.21	0.25

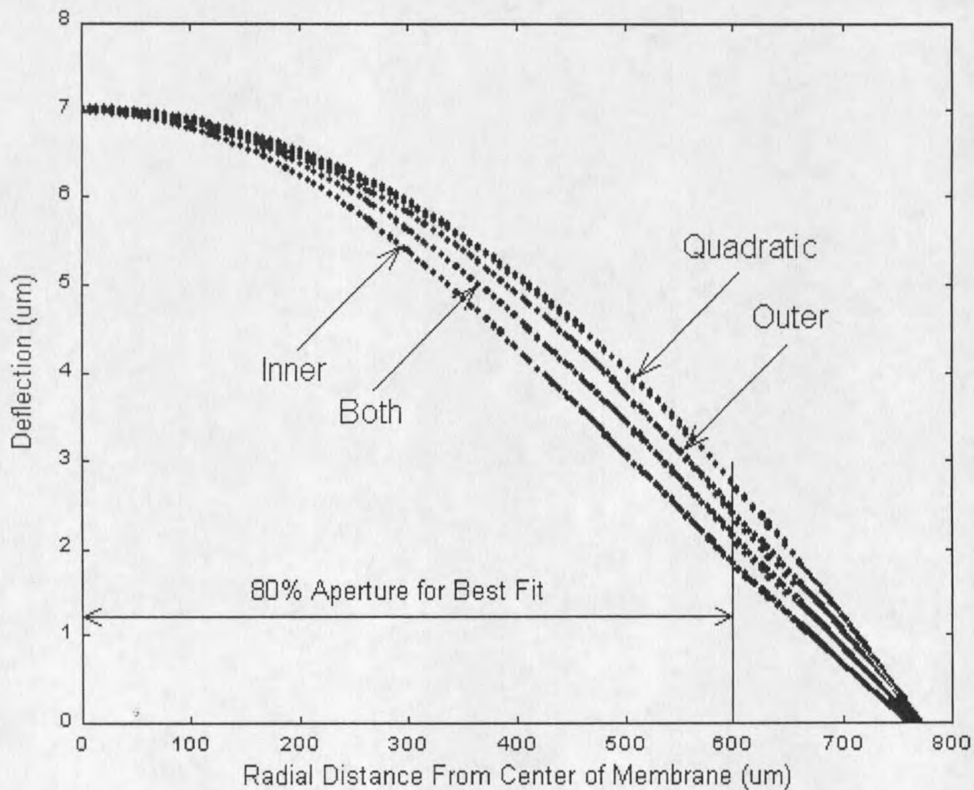

Figure 2-6. FEA Simulation results from actuation of 1500μm device by pressure on inner, outer, and both actuation zones.

FEA simulations also showed that a plate model with an annular thinning of the edge support resembles the behavior of a mechanical membrane (making it act more like a simply supported plate than a clamped plate).

CHAPTER 3

DESIGN

Material / Structural Choices / Fabrication Constraints

The device we are proposing to build is a freestanding membrane on the order of 1000μm diameter with a surface possessing good optical properties, capable of a range of motion of a few microns. As the membrane is deflected, it is desirable that it maintains a parabolic shape, so as not to introduce aberrations to the optical system (as discussed in chapter 2). In previous work [10], oxide was used as a sacrificial layer underneath a polysilicon surface membrane with a single actuation zone. Etching the oxide forms an air gap to allow deflection of the membrane. This conventional polysilicon surface micromachining process is limited to relatively shallow pits underneath the membrane when the devices are released (around 2 microns) because of the long times required for oxide deposition and the quality of the deposited films. A new process was proposed that forms a membrane of silicon nitride rather than polysilicon, which makes it possible to etch the substrate silicon to create an air gap underneath a silicon nitride (Si_xN_y) membrane. By creating a larger gap under the membrane, a greater range of motion can be attained and a larger amount of focus control can be achieved. The process is a hybrid between bulk micromachining (where the bulk of the wafer is etched) and surface micromachining (where layers are deposited on the surface of the wafer and make up the

device). The cross-sectional pictures of the two different methodologies in Figure 3-1 illustrate the difference in range of motion of the different membranes.

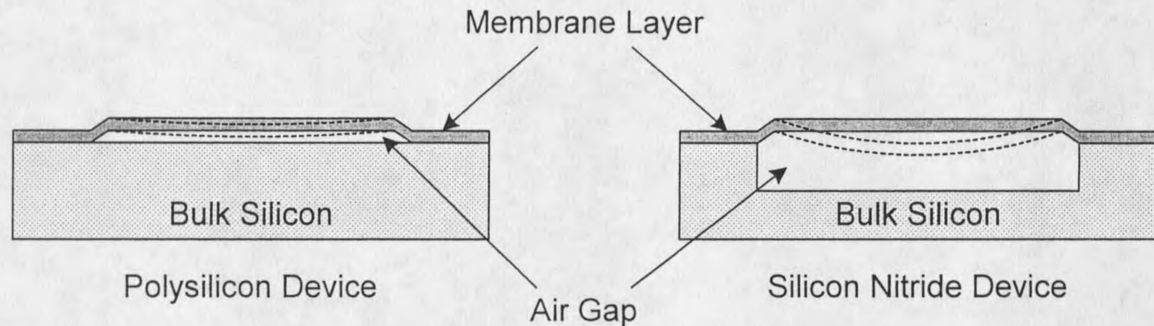

Figure 3-1. Conceptual cross-sections of polysilicon device (surface micromachining) and silicon nitride device (hybrid between surface and bulk micromachining).

Silicon nitride is a material with good mechanical and optical properties, and is also unaffected by the silicon etchant and insignificantly affected by the silicon dioxide etchant. The structure has two metal electrodes on top of the membrane that serve as reflective surfaces as well as a means of deflecting the membrane.

Proposed Device

Based on the discussion in the previous chapter, it is clear the surface profile of the deflected membrane needs to be parabolic in order to achieve focus control while maintaining an aberration-free imaging system. In order to achieve a parabolic shape during deflection, some means of surface shape control need to be implemented. The actuation zones and the boundary conditions of the membrane are areas that need to be addressed in order to control the surface profile once the materials of the membrane are chosen.

Boundary Conditions In order to investigate the effect of boundary conditions on the surface shape of the devices, several variations of edge support were implemented. Each membrane device was designed with two different types of edge support, continuous edge support and segmented edge support with 10% duty width. For devices with circular geometry and segmented support, this implies that 36° of the total 360° of the support consists of silicon nitride. The segmented edge support consists of equally distributed strips with widths on the order of 10 μm. The segmented edge support requires a lower actuation voltage as compared to its continuous edge support equivalent as it has 90% less material that needs to be deformed at the perimeter of the device. This implies that the membrane will achieve a greater range of deflection with the segmented configuration than with the continuously supported version, using the same actuation voltage. As the actuation voltage approaches the maximum for the structure (dictated by the breakdown voltage of the actuation pads), the deflection of the segmented device will be greater. However, the continuously supported device will have better frequency characteristics as its support is more rigid.

In order to improve the curvature profile and lower the actuation voltage, a second method for weakening of the edge support was introduced. The weakening consists of a 9 μm wide trench in the middle of the edge support portion of the membrane, resulting in thinner material at that point. Figure 3-2 shows the conceptual design layout of a 300μm circular device with weakened (thinned) support and segmented edge support. The

weakening of the edge support is displayed as lines across the support where the edges of the thinner portion of the support are located.

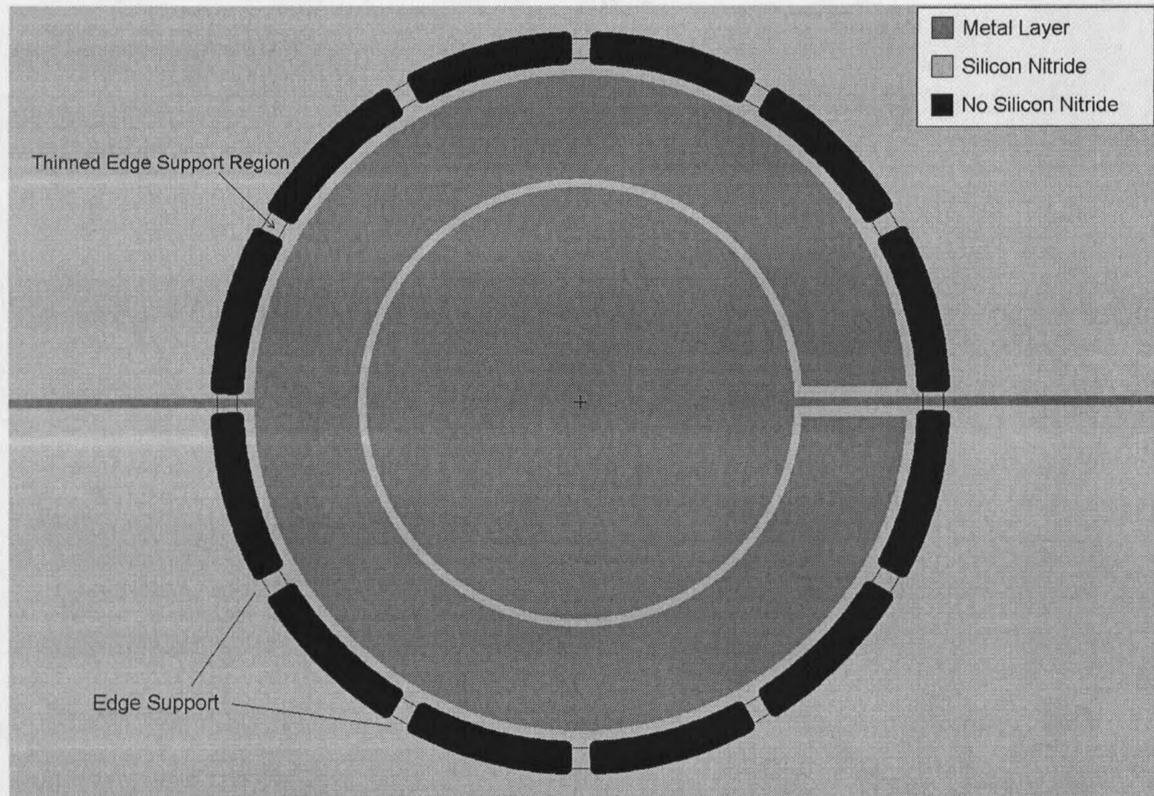

Figure 3-2. Design layout of a 300 μm diameter device with 10% duty width and weakened edge support.

Actuation Regions In order to deflect the membrane, a metal layer is deposited on top of the membrane. This layer acts as a reflective surface as well as a means to deflect the membrane. By applying a voltage potential to the metal layer and grounding the substrate (bulk silicon of wafer), a voltage potential difference is established between the membrane and the substrate. An electrostatic attraction between the membrane and the bulk material will arise and the membrane will deflect towards the substrate. In order to achieve greater control of the surface profile of the membrane devices, a scheme using two different actuation zones was introduced. The actuation zones consist of two metal

regions (layered chromium/gold films) on the membrane, separated by a minimum lateral distance of 5μm to prevent arcing between the different voltage potential zones. The actuation zones of the circular devices consist of a circular center actuator and an outer annular actuation zone. An example of these actuation zones is shown in figure 3-2. Since the two regions are separated from each other, it is possible to control the surface shape of the membrane by applying different voltages to the two actuators. Since, radially, the inner electrode is twice the size of the outer electrode and is located in the middle of the membrane, it is clear that the inner electrode will have a greater impact on the amount of deflection achieved. The outer electrode will also affect the amount of deflection achieved, but its main role will be to control the overall surface profile of the membrane as it is located at the edge where the membrane is anchored. The role of each of the actuation zones in the surface shape of the membrane will be investigated in chapter 5. By creating a lookup table of the relationship between the inner and outer electrode voltages and the resulting surface shape of a device, a computer can be used to control the voltages of the actuation zones and thereby maintaining zero spherical aberration at different levels of focus control (by canceling the r^4 term of the surface shape, as discussed in chapter 2 and chapter 5).

Etch Holes In order to etch a pit underneath the silicon nitride membrane, means for the wet etchant to reach the material underneath it need to be provided. By introducing a grid of small holes (on the order of a few microns in diameter) into the membrane structure, the liquid etchant can reach the layers underneath the membrane. In the case of devices

with segmented support, there are large holes (approximately 50 times the size of the etch holes) present at the edges of these devices. The liquid etchants will therefore gain better access to the materials under the membrane of these devices, as it is not limited to only using the etch-holes as with the continuously supported devices. Therefore, the spacing and size of the etch-holes play a vital part in the design of the continuously supported devices.

Secondary Concerns

There are a few secondary considerations of the design that need to be considered. By making the pit depth larger, the actuation voltage needed to deflect the membrane gets larger. If the pit depth is too great, the voltage needed to deflect the membrane might be too large for the device to work (see chapter 4). During the fabrication of the device, Hydrofluoric Acid (HF) and Tetramethyl Ammonium Hydroxide ($(CH_3)_4NOH$, TMAH) is used to etch the oxide and the silicon respectively. Special consideration has to be observed as the HF attacks the silicon nitride as well as the oxide, for which it is intended. Furthermore, silicon etching generates hydrogen bubbles, which must be considered during design as they might cause the membrane to fail if the etch is too violent for the structure. The amount of deflection for a certain voltage will differ with device size and type of edge support, therefore the optimal pit depth differs for each device.

Final Device Idea

The completed device is a freestanding silicon nitride membrane with a metal layer acting as reflector and actuation zone. There are two different actuation zones and by applying different voltage potentials to the two zones, surface profile control is achieved. The devices have a grid of small etch holes, which enables the chemicals in the release step to reach the underlying layers. The membranes are made with two different edge support versions, continuous support and segmented support. The devices with segmented support require a lower voltage than their continuously supported counterpart to achieve the same level of deflection. Weakening of the edge support is an option that will give a better surface profile when actuated (and require a lower actuation voltage). The weakening of the edge support consists of a trench in the supporting silicon nitride structure. In order to be used in a wide range of applications and enable troubleshooting of the release process, devices of varying size and edge support configurations were produced on the same die (smallest part of wafer, containing all device variations). All devices on the die are made both with segmented edge support and without. The circular devices were manufactured with diameters of 300μm, 750μm, 1mm, 1.25mm, and 1.5mm.

CHAPTER 4

MAKING THE DEVICES

Process Flow

The membrane surface micromachining process is divided into two main parts:

- Fabrication at the nanofabrication facility at Stanford University (by Ph.D. candidate Phillip A. Himmer [dissertation to be published in 2001]).
- Postprocessing (Release) at Montana State University.

The initial fabrication step is where the different layers are deposited, patterned, and etched. In the release step, the membrane layers are etched away from the surrounding material layers and become a self-supporting device.

The micromachining process for a device is as follows:

1. A trench is etched in the bulk material of the silicon wafer, forming a perimeter about the area where the final device will be located. This trench serves as a lateral etch stop and prevents undercutting of the device.
2. A nitride layer is deposited which backfills the lateral etch stop trench. Nitride is then removed everywhere (no mask used in order to reduce surface roughness over trench).
3. A 0.7 μm thick phospho-Silicate Glass (PSG) (8% phosphorus) oxide layer is deposited where the device is to be machined. During release, this oxide layer is etched first, forming a gap between the membrane and the silicon substrate. This

enables the silicon etchant to reach the underlying silicon and etch a flat pit bottom under the membrane (once the oxide is etched away).

4. If a thinned edge support is desired, a nitride layer is deposited and then patterned/etched where the weakening will exist. This step controls how deep the weakening trench will be with respect to the entire membrane structure.
5. A nitride layer is deposited which makes up the nitride membrane structure. In the case of a device with thinned support, this step defines how thick the thinned support region will be. The membrane thickness will be the sum of the depositions in steps 4 and 5.
6. Metal layers are deposited, patterned, and etched. A thin chromium layer (50Å) is deposited first as an adhesion layer for the gold layer (1000Å), which makes up the reflective surface/actuation region.
7. Etch holes are patterned and etched in the metal layers.
8. Etch holes and support definition openings (for the devices with segmented support) are patterned and etched in the nitride membrane structure.
9. Release step:
    - Oxide is etched away under membrane structure.
    - Silicon is etched away under membrane structure.

Figure 4-1 shows the described fabrication sequence of the membrane devices.

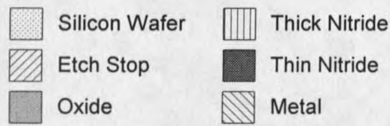

Etch 2 μm wide Trench (Lateral etch stop). Deposit LPCVD Silicon nitride to backfill. Remove nitride from surface using RIE etch.

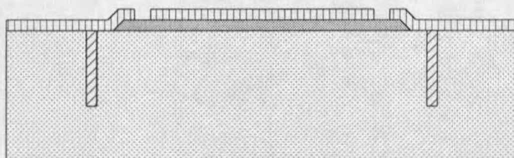

Deposit and pattern 1 μm thick PSG (Oxide) plate. Deposit 0.5 μm thick Silicon Nitride (Thick Nitride), etch thinned support region (if so desired)

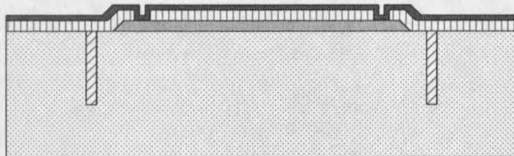

Deposit 0.5 μm thick Silicon Nitride (Thin Nitride)

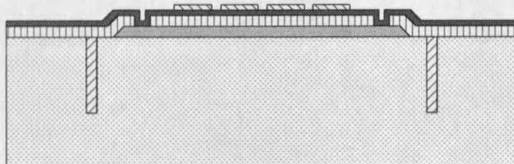

Deposit, pattern and etch Metal Layers (50 Å Cr, 1000 Å Au).

Pattern and etch segmented support and etch holes in Silicon Nitride.

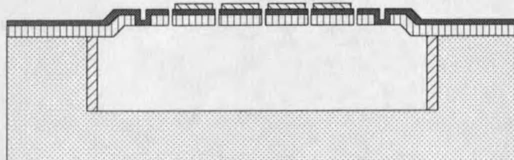

Release: Etch Oxide in HF. Etch Silicon in TMAH or KOH.

Figure 4-1. Fabrication sequence for the membrane mirrors.

Considerations When designing the devices, a process flow had to be fashioned where the underlying layer is protected from the deposition, patterning, and etching of the subsequent layers. The process has to take into account what each subsequent layer will do to the previously deposited layers and ensure that the process flow will not damage the previous layers or lead to undesired undercutting of structures (at time of deposition or during subsequent depositions/etches). The main considerations of the membrane mirrors (assuming fabrication is ideal) are their optical quality, and ensuring that the edge supports are not undercut and thereby causing a non-parabolic surface during deflection. The surface shape of a membrane under uniform pressure is dependent on the boundary condition of the device [4]. Consequently, if the boundary is not circular, the surface shape of the deflected membrane will be non-parabolic. Due to the crystal structure of silicon, if no etch stop is present, the pit etched from a circular opening will be square (if the etch progresses for some time). If the etch progresses for a long time, the resulting pit will be an inverted pyramid. Since the pits being etched beneath the membrane devices are relatively shallow compared to the diameter of the openings, the inverted pyramids do not have time to form. Figure 4-4 d) shows an image of a square device with sloping side-walls due to this effect. Since the pit is shallow compared to the overall device size, the sloping side-walls are located under the support part of the device and do not interfere with the operation of the device.

Layout The layout tool used for generating the masks was Tanner Tools L-Edit. The masks were made with a smallest feature size of 3 μm, and a minimum lateral feature size of 2 μm (1 μm between via hole layers). The membrane mirror design consists of 6 different mask layers (in order of lithographic steps):

1. Silicon etch layer for lateral etch stop
2. Oxide pad definition layer
3. Silicon nitride thinned edge support definition layer (optional)
4. Metal layer
5. Metal etch hole layer (No way of merging layers 4 & 5 in L-Edit)
6. Nitride etch holes and segmented support

Figure 4-2 shows the different mask layers discussed above. From figures 4-1 and 4-2, it can be seen that some of the layers represent where material will be deposited, and others show where material will be left out of the deposited layer.

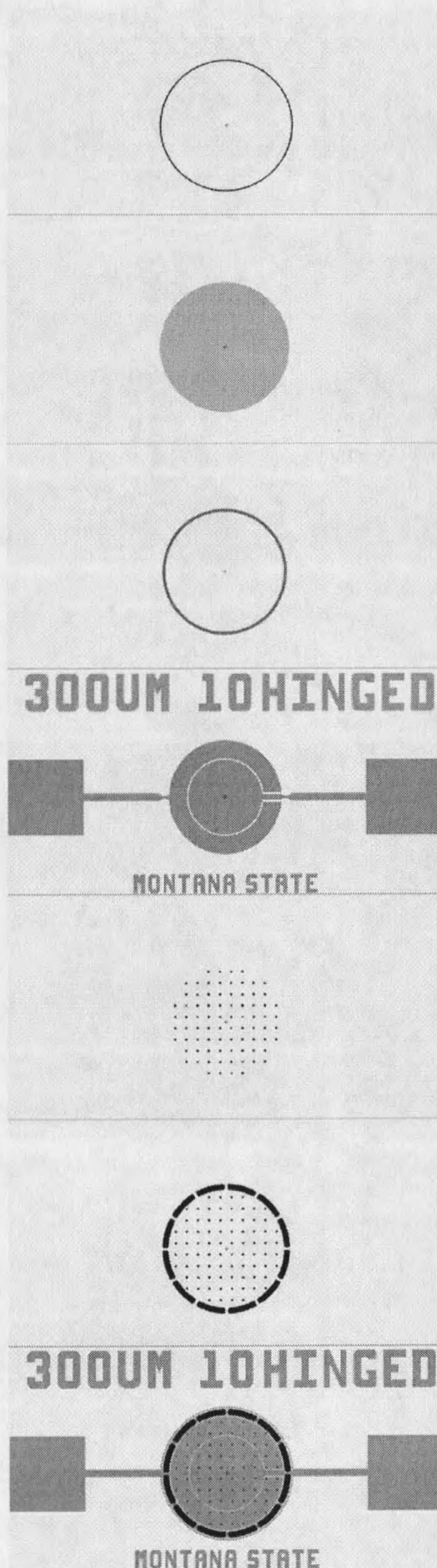

Trench etching mask for lateral etch stop in silicon wafer (surrounds devices according to their geometry).

Oxide pad mask (provides etch stop for thinned support definition etch and easier access for silicon wet etchant during release).

Thin support definition mask (etches trench in first deposited silicon nitride layer).

Metal mask for deposition of Chromium (adhesive layer) and Gold (actuation zones / reflective surface) layers.

Metal via etch mask (due to limitations in the layout software, this layer could not be merged with the previous metal layer).

Nitride via and segmented support definition layer.

Final layout of device (all layers included).

Figure 4-2. Mask Layers of the membrane mirrors.

Figure 4-3 shows an image of a released (freestanding) 1500μm 10% device without thinning of the edge support. Imperfections of the device in the picture are caused by dust on the die.

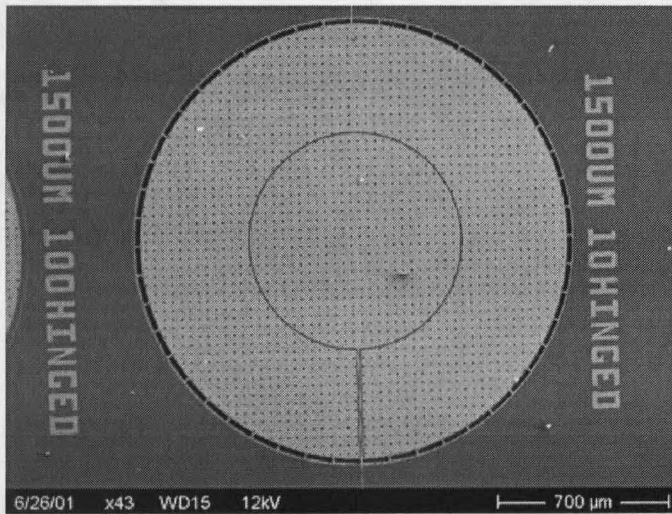

Figure 4-3. SEM picture of 1500μm device with segmented but no thinning of the edge support.

In figure 4-4, SEM images of released devices show what the final structure looks like. The lateral etch stop is shown on the left side of a). The cross-sectional image shows where the nitride is pinched off at the top and leaves an outline on the top surface of the structure. A metal trace going across a back-filled etch stop trench is shown in b). The image further shows the outline the back-filled etch stop trench leaves on the top surface of the device. The thinning of the edge support and the raised edge outline the oxide pad leaves in the membrane structure is shown in c). A broken square device with thinned and segmented edge support is shown in d). It can be seen that the sidewall next to the lateral etch stop is not straight. The sloping sidewalls of the pit beneath the square device are

caused by different etch selectivity to the different crystal planes of silicon by the silicon etchant (some crystal planes etch slower than others) [13].

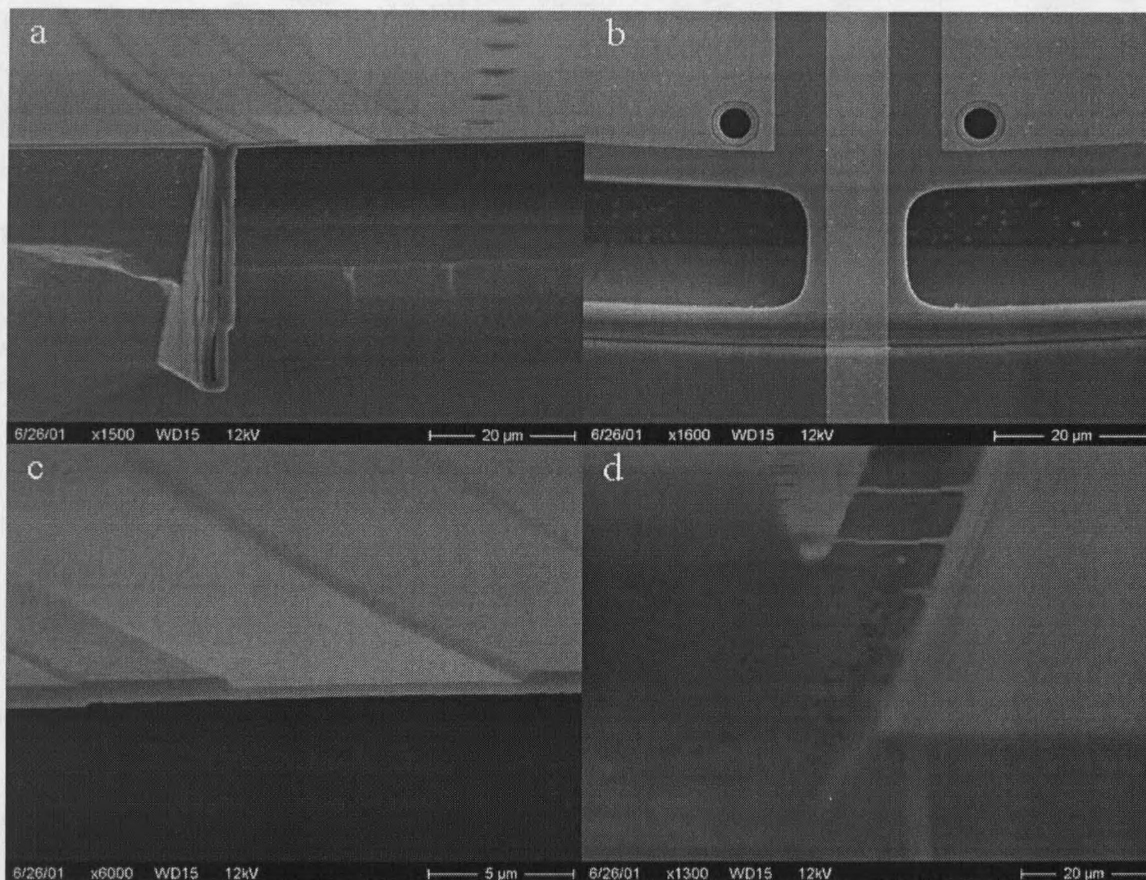

Figure 4-4. SEM images of membrane devices illustrating key features.
a) Lateral etch-stop and thinned support of circular device.
b) Metal trace crossing back-filled etch stop trench.
c) Close-up of thinned edge support.
d) Segmented thinned support of broken square device.

Release Process

Wafers were received at MSU with the previously mentioned processing completed. Many times, the final layer of photoresist is still present on the wafers. To strip the photoresist off the wafers, either Acetone or Piranha (3:1 Sulfuric Acid : Hydrogen

Peroxide [H_2SO_4:H_2O_2]) can be used. Piranha was the mixture of choice as it also removes most other organic residue (and works more rapidly). When etching the PSG Oxide, HF (Hydrofluoric Acid), or BOE (Buffered Oxide Etch) can be used. For the nitride devices a fresh batch of 3:1 HF (52-55%):H_2O solution was used for each die as this concentration gave good yields, short etch times, and still maintained excellent selectivity (Oxide vs. Nitride). For etching silicon, there are a number of anisotropic wet-etchants available. For the membrane mirrors, KOH (Potassium Hydroxide in an H_2O solution) and TMAH (Tetramethyl Ammonium Hydroxide) were the main etchants used.

Considerations When etching, there are several things to consider. Concentration, temperature, etch selectivity, and etch-time are the main factors. After investigating the interaction between etch parameters, a final release process was conceived.

Cleaning Die: 15 minutes in Piranha at 70 °C (readout of hotplate).

Etching PSG Oxide: 15 minutes in a fresh batch of 3:1 HF (giving a final HF concentration of 13% - 13.75%) at room temperature.

Etching Silicon: ~2 hours in TMAH (10% solution by weight) at 50 °C (hotplate readout).

In the process used to manufacture the membranes, when it comes time to etch the PSG oxide, HF has access to gold, edges of chromium, nitride, and silicon. HF does not etch gold, chromium, or silicon at all and has a very high etch selectivity when compared to silicon nitride. By using a profilometer and microscope respectively, it was found that in 3:1 HF solution the lateral etch rate of oxide underneath the membrane is 2.83 μm/minute

and the nitride etch rate is 11 Å/min, which means 3:1 HF has a 2600:1 selectivity (lateral vs. planar). This shows that when the oxide is etched (15 min etch time), the nitride membrane is weakened by 16.5 nm from both sides of the membrane (as the bottom gets exposed). Devices with thinned edge support were made that had a center membrane thickness of 1μm and a thinned edge support thickness of 0.5 μm. The thinned region of the edge support of the membrane is thereby further thinned by 6.6% when the oxide is etched.

TMAH does not etch anything on the membrane structure but the silicon, which makes it an ideal silicon etchant. When etching the bulk silicon of the wafer, the etch-time depends on the desired pit-depth underneath the membrane or vice-versa. The desired pit-depth depends on which device on the die is of interest (dictated by actuation constraints such as breakdown voltage and device size and type). TMAH etching of silicon has its peak around 2-5% concentration, depending on silicon characteristics [14, 15]. It was found that 10 % TMAH concentration gives good yield and has a reasonable etch rate. Typically, with the etch hole configuration of the membranes (3μm diameter, 30 μm spaced grid), two hours in TMAH (10 % solution) at 50 °C (hotplate readout) will give a pit depth of approximately 13 μm. For the larger devices (1mm and above), a pit depth of 10-15 μm is desired as it will produce deflections on the order of 1-3 μm (as specified in chapter 2) for voltages under 200V and have enough clearance underneath the membrane to keep it within stable operation. Stable operation can be defined as the range of motion of the membrane where the electrostatic force is smaller than the

restoring force of the membrane structure, keeps the membrane from snapping down to the substrate of the die.

If the needed actuation voltage for a certain level of focus control is high, the possibility of reaching the breakdown voltage of the actuation pads arises. The breakdown voltage is the point at which current flows through the silicon nitride layers from the top layer metal to the underlying silicon (the counter electrode). By monitoring the electrode current, it is possible to determine whether breakdown is imminent. An experiment was conducted on a contact pad that was not connected to a membrane. It was found that the current has an exponential characteristic and for the given thickness of the layers, significant current was observed for voltages above 150V (Figure 5-12).

When devices are released, the devices with thinned edge support have a low yield. The 300μm devices have yield above 95% but the larger devices are rarely intact. It seems that 0.5μm thickness for the thinned edge support region is not thick enough, as the larger devices have such a low yield. Comparing the two different edge support alternatives of the thinned support devices shows that segmented edge support devices have lower yield than continuous edge support devices.

Devices without thinning of the edge support have higher yield. The membranes have a uniform silicon nitride thickness of 1μm across the devices, which gives a more robust structure. The 300μm devices have a yield greater than 95%, and the larger circular devices have a yield of above 50%. As with the thinned devices, segmented edge support devices have lower yield than continuous devices.

Imaging of Release Process To investigate why devices are breaking during the release step, a lens system (Navitar Zoom 6000) with a long working distance (9 cm) and a small field of view (down to <300 μm) was acquired. The system was used to image the Oxide etch and the Silicon etch as devices are failing during both steps. To protect the lens-camera system, it was encapsulated in a layer of nitrile rubber. The system was mounted on a ringstand for flexibility. The imaging process of the two etches is different due to the nature of the chemicals and the etch process itself. During the Silicon etching, hydrogen bubbles are formed [14] that makes imaging from the top impossible (condensation on the glass surface is also a factor). Here, the die is placed in a holder and the etching is imaged through the sidewall of a square box made out of Pyrex glass. The setup for imaging during Silicon etching is shown in figure 4-5. The major issues during the imaging process are the illumination of the devices of interest and the reflection off the fluid or the side of the beaker. Since HF etches glass, it can not be imaged through the sidewall of a glass beaker, instead it has to be imaged from above in a beaker which is resistant to the chemical. To protect the lens system from the fumes of the HF in the plastic beaker below, a glass window is placed at the front of the lens system. As the byproduct of HF etching of Oxide is water [15], no bubbling occurs when the oxide is etched (field of view of 300um) and it is therefore possible to obtain a good image from above. The lighting is however an issue, as the light has to come from above and reflects off the sides of the beaker. The lens system has a coaxial illuminator that can be connected by a fiber bundle to a light-source; alternatively semi-rigid gooseneck light

guides can be used to provide diffuse illumination. Proper illumination takes some time to set up and therefore images of the initial part of the etching sequence are hard to acquire.

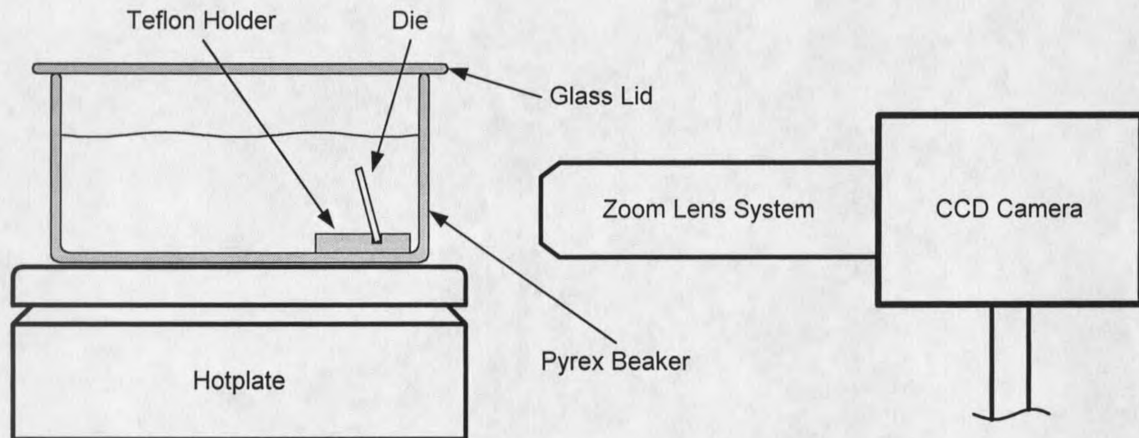

Figure 4-5. Setup for imaging of silicon etching process.

Results Oxide Etch While etching the oxide in HF, there are some devices that are failing. By using a fresh batch of HF for each die, the survival rate increased. Devices with thinned support have a lower survival rate than the ones without (the devices are failing at the transition region between the thinned support and the full thickness membrane structure). Figure 4-6 shows a SEM image of a cross-section of a square device where the thinned edge support has broken off at the two transitions to thinned edge support.

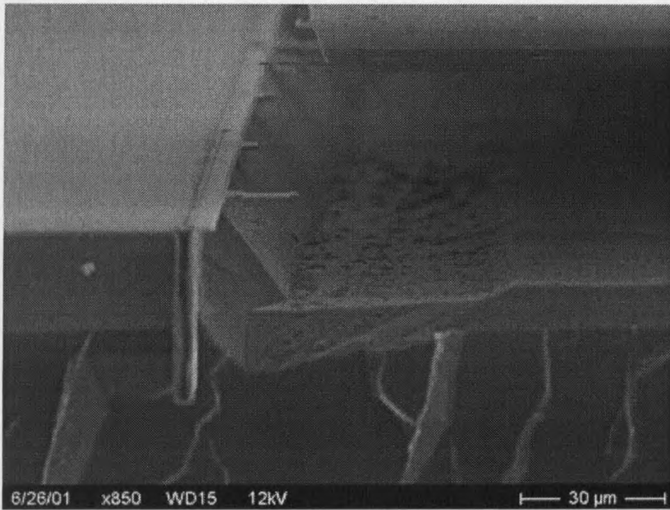

Figure 4-6. SEM image of broken device, illustrating where devices with thinned edge support break.

The devices do not always break at the edge; they can also fracture from pressure. Figure 4-7 shows an example of such a crack. The crack goes through the nitride, chrome, and the gold layers and terminates in a via hole as the stresses are small there.

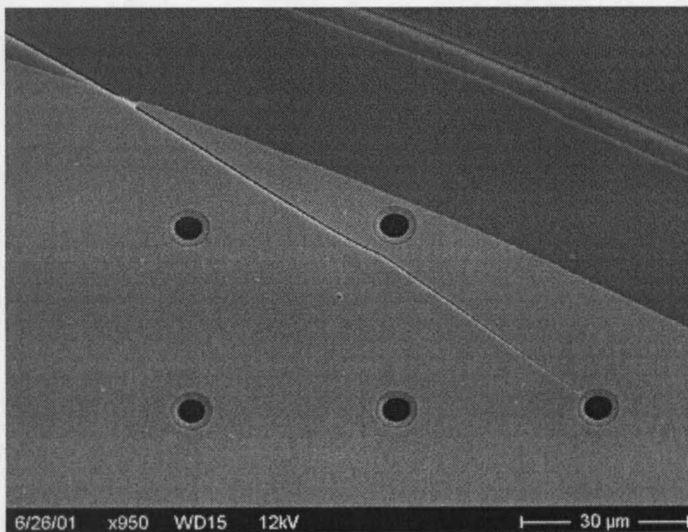

Figure 4-7. Crack in membrane structure terminating in etch hole.

With the devices that have no thinning of the edge-support, most of the devices are surviving the oxide etch, but the largest devices (2mm elliptical and 2x1mm square) are still not making it through the silicon etch. It was found that, when the gold and chrome

layers are etched away on devices with no thinning of the support, the devices are surviving the oxide and silicon etch steps. The conclusion is that the tensile stress of the metal layers is pulling the devices apart as soon as they become freestanding.

The anisotropic etching process of the oxide etches through the grid of etch holes (and the openings at the edges for the devices with segmented support). Each etch hole gives rise to a bowl shaped pit underneath the membrane and when the bowl shaped etch fronts reach the underlying silicon, it acts as an etch stop and the etch fronts only progress laterally. When the etch fronts meet, pillars are formed between the etch holes. At the moment when the pillars are starting to etch away completely, a "wave" of collapsing pillars is observed moving across the wafer (the entire sequence lasts a few seconds). Figure 4-8 shows screen-captures from an oxide etch process of a 1000μm 10% device at the time the wave is propagating across the membrane. In a), the wave has just started at the perimeter. The wave reaches the center actuation zone in b) and has moved to the center of the devices in c). The device is freestanding in d). In all pictures of figure 4-8, the periodic bright and dark sections at the perimeter are caused by the segmented edge support. The dark parts are where there are nitride strips and the bright parts are due to a small buckling of the membrane between these strips. The periodic pattern is visible in all frames of figure 4-8 because the edges are being etched from the start due to the openings at the perimeter and become freestanding before the rest of the device. The cause of the dimples on the membrane of figure 4-8 is not clear. When the HF etch was over, the die was placed in water and the location of all dimples on devices on the die were mapped. The die was inspected after the silicon etch and it was found that the dimples did not have

an impact on where devices broke. The cause of the dimples is unclear, but they could be formed by stiction to the bottom of the device.

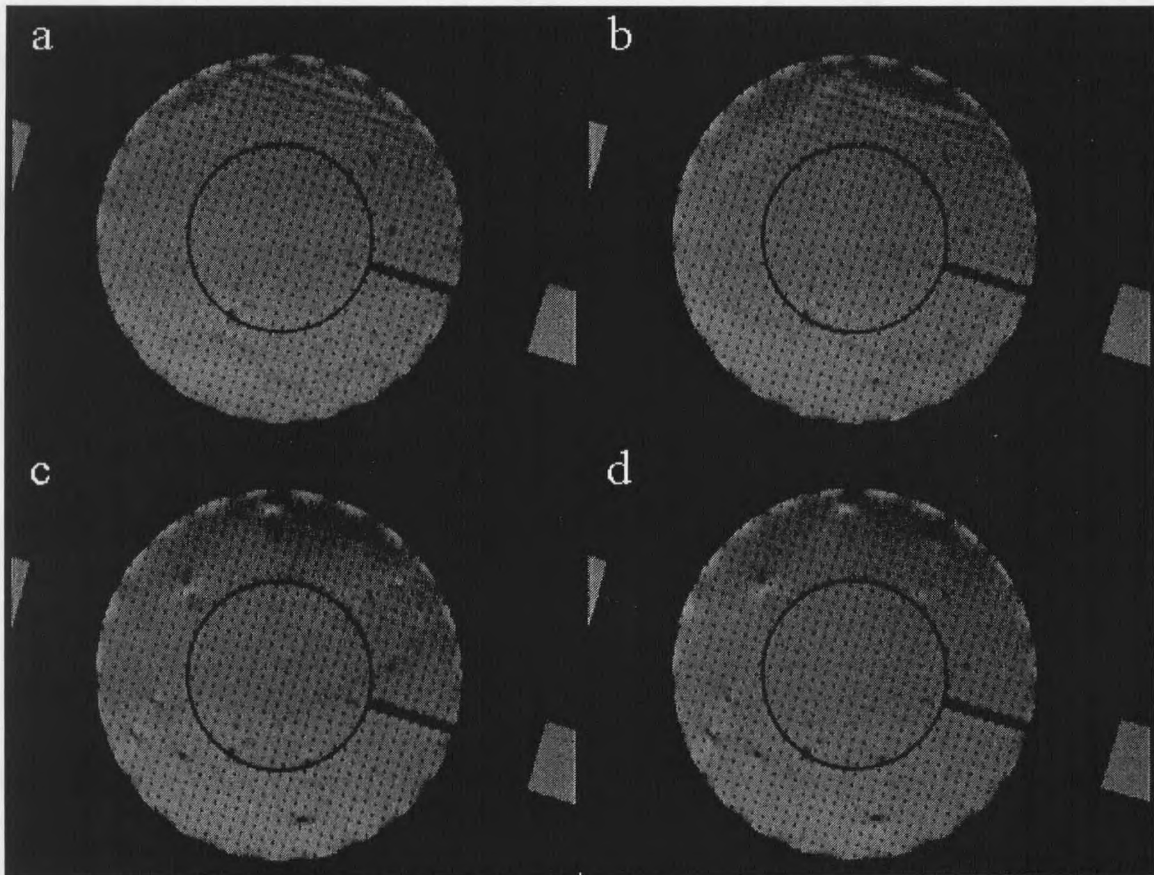

Figure 4-8. Wave propagating across 1000μm 10% device as pillars beneath membrane are etched away.

a) Wave propagates from perimeter of device.
b) Wave reaches center actuation zone.
c) Amount of remaining pillars is less than diameter of center actuator.
d) Device is freestanding.

Larger devices (1000μm and larger) with thinned edge support rarely make it intact through the HF etch step. To investigate the effect of HF concentrations on device survival rates, an experiment where dies containing devices with thinned edge support were etched in HF was conducted. The concentrations were 3:1, 4:1, and 5:1. No apparent variation in yield was displayed.

Results Silicon Etch While etching the silicon under the membrane, hydrogen gas is formed as a byproduct. By stripping the metal layers off the nitride membrane, it is possible to see how the larger bubbles are formed and how they exit from underneath the membrane. It seems logical that a steady stream of bubbles would come out of each of the etch holes (vias) if the bubbles forming are small enough. After imaging several of these processes, it is clear that this is not always the case. Most of the time, there will be a steady stream of bubbles coming out of a few of the vias. Sometimes the bubbles will keep coming out of the same vias for a long time and then switch to other etch holes and then occasionally back again. Underneath the devices with continuous support, the bubbles sometimes start as a steady stream of bubbles coming out of a few etch holes. Then the stream of bubbles will stop and a large bubble will start to form in the middle of the device and expand out to the perimeter and when enough pressure has been built up, one out of two things will happen:

- The bubble will release the gas by explosive bursts of small bubbles through what appears to be most of the vias at the same time.
- The burst of bubbles will break the device and continue bubbling from the cracked edge of the device. The device will most likely break at the edge. In the case of the thinned edge support, the device will most likely break.

As it does not seem possible to image through the membrane onto the bulk silicon when the device is in TMAH, it is hard to make any predictions as to why the bubbles form in the manner they do. Figure 4-9 shows frames from a video of the described bubbling behavior (up is to the left of the images). The images show a 1500μm continuously

supported device without thinning of the edge support etching in 10% TMAH solution at a temperature of 50°C. As shown, the bubbles start out as a steady stream in a). The stream then cease in b). Pressure builds up beneath the membrane in c). The bright spot at the top of the membrane indicates a buckling of the device since the lighting conditions remained the same during the filming and there was no bright spot at that location in before (b)). The pressure is then released by an explosive burst of bubbles in d).

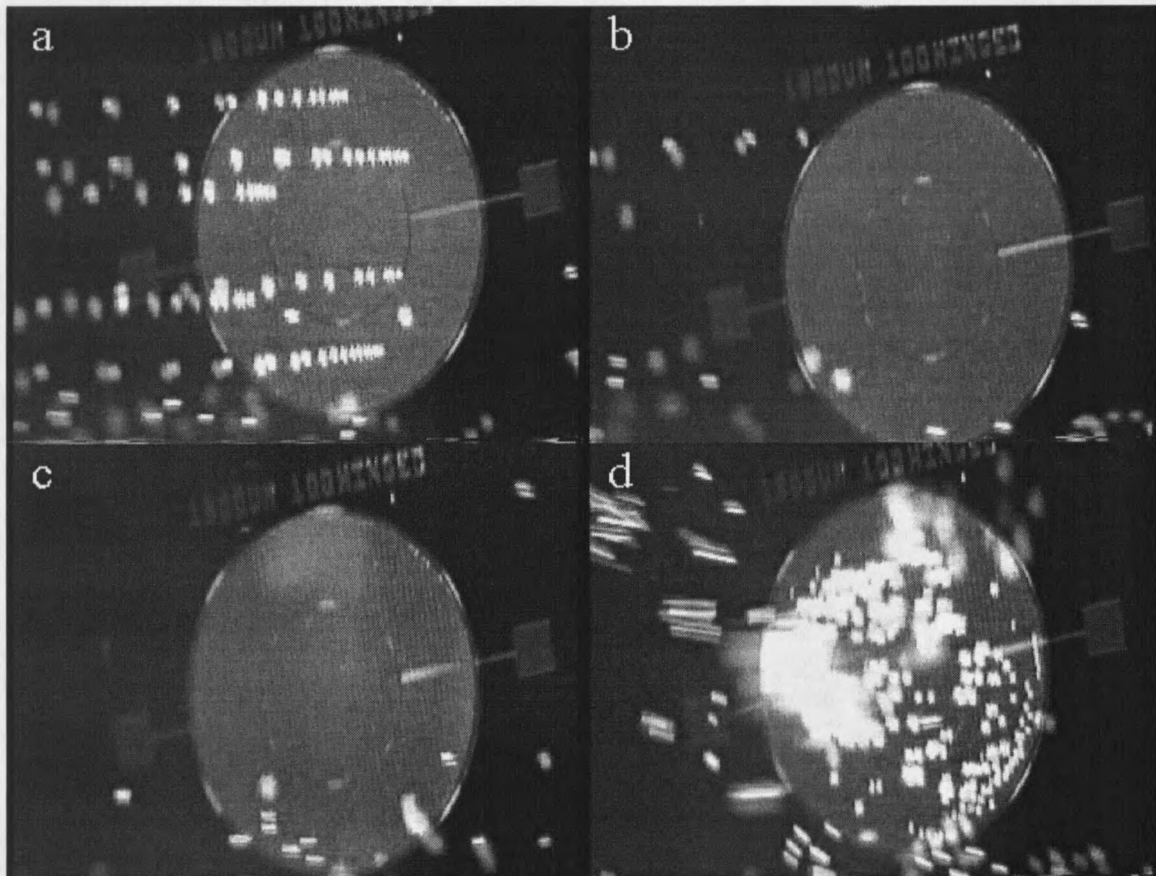

Figure 4-9. Frames from video of TMAH silicon etch (up is to the left).
a) Steady stream of bubbles coming out of a few vias.
b) Stream of bubbles cease.
c) Large bubble is forming beneath membrane.
d) Explosive burst, releasing hydrogen bubbles.

On a wafer where devices have no thinning of the edge support, there are no visible bubbles forming from some devices in the Silicon etch, even though bubbles are forming at sides of die where silicon is exposed. There is no explanation why this occurs, as the devices with the continuous support were manufactured in the same batch as the ones with the thinned supports and these devices have clearly visible bubbles coming out from under the membranes. The only thing differing in the manufacturing of the two wafers was that the wafer with the thinned support had an extra patterning/etching step where the thinned support pattern is deposited and then the nitride was etched away.

In an attempt to increase device yield, isopropanol (2-propanol, IPA) was added to the TMAH solution. This was done in order to decrease surface tension in the solution. IPA was added until the 10% TMAH solution was saturated. The bubbles forming were smaller and not as plentiful as for the 10% solution. As the etch progressed, the stream of bubbles decreased and was found to have etched a mere 3μm after an hour at a temperature of 50°C.

The bottom of the devices vary depending on whether the device has continuous or segmented edge support. Figure 4-10 shows what the bottom surface of the two variations of devices looks like. For the segmented support, the silicon etchant has better access to the surrounding chemical and it therefore etches more rapidly at the edge and leaves a deeper ring in the silicon at the edge (approximately 3μm deep). Since the only access the continuous device has with the TMAH is through the vias, the etch is more uniform and leaves a flat bottom across the entire device.